

Identifying Reliable Predictions in Detection Transformers

Young-Jin Park*, Carson Sobolewski*, and Navid Azizan

Massachusetts Institute of Technology

{youngp, csobo, azizan}@mit.edu

Abstract

DEtection TRansformer (DETR) has emerged as a promising architecture for object detection, offering an end-to-end prediction pipeline. In practice, however, DETR generates hundreds of predictions that far outnumber the actual number of objects present in an image. This raises the question: can we trust and use all of these predictions? Addressing this concern, we present empirical evidence highlighting how different predictions within the same image play distinct roles, resulting in varying reliability levels across those predictions. More specifically, while multiple predictions are often made for a single object, our findings show that most often one such prediction is well-calibrated, and the others are poorly calibrated. Based on these insights, we demonstrate identifying a reliable subset of DETR’s predictions is crucial for accurately assessing the reliability of the model at both object and image levels.

Building on this viewpoint, we first tackle the shortcomings of widely used performance and calibration metrics, such as average precision and various forms of expected calibration error. Specifically, they are inadequate for determining which subset of DETR’s predictions should be trusted and utilized. In response, we present Object-level Calibration Error (OCE), which is capable of assessing the calibration quality both across different models and among various configurations within a specific model. As a final contribution, we introduce a post hoc Uncertainty Quantification (UQ) framework that predicts the accuracy of the model on a per-image basis. By contrasting the average confidence scores of positive (i.e., likely to be matched) and negative predictions determined by OCE, the framework assesses the reliability of the DETR model for each test image. The code is available at <https://github.com/azizanlab/reliable-det>.

1. Introduction

Object detection is an essential task in computer vision, with applications that span various domains including autonomous driving, warehousing, and medical image analysis. Existing object detection methods predominantly utilize Convolutional Neural Networks (CNNs) [8, 9, 22, 23] to identify and locate objects within images. However, the recent introduction of DEtection TRansformer (DETR) [1] has revolutionized the field by offering an end-to-end prediction pipeline where the model predicts a set of bounding boxes and class probabilities.

The core innovation of DETR lies in the use of a Transformer encoder-decoder architecture, enabling the model to generate predictions in an end-to-end manner and enhancing scalability. This paradigm shift has led to the exploration of various DETR variants—such as Deformable-DETR [32] and DINO [31]—positioning them as potential foundation models for object detection tasks. Despite these advancements, the inner workings of how these predictions are generated and interact within the Transformer decoder layers remain under-explored.

Likewise, there is an ongoing debate within the community about whether DETR truly provides an end-to-end prediction pipeline. The central concern is *whether all the hundreds of predictions generated by DETR can be trusted and used*. By means of an answer, practitioners often employ heuristic approaches to achieve high precision, such as by setting a user-defined threshold to retain only a small subset of high-confidence outputs, as seen in the official [demo](#). Previous studies exploring model reliability, such as [10, 15–17, 21], have also applied a user-defined confidence threshold (e.g., 0.3) to retain a subset of predictions for evaluating calibration quality, rather than using the entire set. On the other hand, the published implementations of several DETR variants select the top- k outputs (e.g., 100 out of 300 for Deformable-DETR and 300 out of 900 for DINO) based on confidence scores during post-processing to achieve a high average precision (AP) score. However, the significance of selecting a subset of the predictions as well as the choice of a suitable configuration for doing so remain under-explored. We provide a more in-depth dis-

*Contributed equally and share co-first authorship.



(a) Low confidence with random boxes

(b) Calibrated confidence with similar boxes

(c) Uncalibrated confidence with similar boxes

Figure 1. DETR generates hundreds of predictions for each image, resulting in multiple predictions per object, with one being well-calibrated. This figure illustrates how DETR can handle the remaining predictions. In principle, DETR may (a) generate low confidence with random bounding boxes, (b) assign equally calibrated confidence with similar boxes, or (c) poorly calibrated confidence with similar boxes. Our analysis indicates that DETR mostly follows the third scheme; resulting in varying levels of reliability across predictions.

cussion about related works in Appendix A.

This paper examines these issues by addressing the following **three research questions**: (RQ1) Do all predictions generated for a given image exhibit comparable levels of reliability? (RQ2) If not, what is the appropriate way to identify reliable predictions across the entire set? and (RQ3) How can we accurately assess DETR’s reliability?

Our primary findings reveal that predictions from DETR within the same image are interdependent, leading to varying levels of reliability. Since DETR is trained using gradients from optimally matched predictions, it has flexibility in handling the remaining predictions. In principle, DETR could assign them low confidence with random bounding boxes (Figure 1a). Alternatively, it could also generate similar bounding boxes with equally calibrated confidence (Figure 1b). Otherwise, it may assign poorly calibrated confidence scores (Figure 1c). Our analysis indicates that DETR mostly follows the third scheme; we refer to these well-calibrated predictions as *positive* predictions and the others as *negative* predictions.

Building on this observation, this paper investigates the importance of distinguishing between positive and negative predictions, and how this finding can be leveraged into an uncertainty quantification (UQ) framework for DETR. More specifically, our main contributions are:

- We offer both qualitative and quantitative insights into how positive and negative predictions influence the model’s object-level calibration. Our analysis shows that negative predictions are poorly calibrated. Furthermore, their confidence scores are inversely correlated with image-level reliability, highlighting the need for a separation method to ensure DETR’s reliable use.
- We raise concerns about existing performance and calibration metrics—including AP [6, 14, 25], detection expected calibration error (D-ECE) [10], and Localisation-aware expected calibration error (LA-ECE) [11, 19]—by noting their inadequacy for identifying the reliable subset of predictions. For instance, AP favors retaining more predictions, while ECE prefers a smaller high-confidence set. Consequently, the subset of predictions that maxi-

mizes performance for each metric differs significantly from the optimal positive set.

- To address this, we introduce a new calibration metric, object-level calibration error (OCE), which calculates calibration error along ground truth objects rather than predictions. We demonstrate that OCE is capable of both ranking different models by their calibration qualities and identifying the reliable subset of predictions to use.
- Based on our findings, we provide a practical implication: we introduce a novel framework for quantifying image-level reliability by contrasting the average confidence scores between the positive and negative predictions identified by our OCE metric. We conduct numerical experiments, demonstrating the effectiveness of our approach across in-distribution, near out-of-distribution, and far out-of-distribution scenarios.
- We present a comparative analysis of methods for identifying positive predictions in DETR, from the UQ perspective. Our results show that thresholding (on predictive confidence score) is a more suitable method than widely used techniques such as top- k or non-maximum suppression (NMS) for obtaining a reliable subset of predictions.

2. Problem Statement

2.1. Detection Transformers (DETRs)

We consider a test image x and denote \mathcal{T}_x as the set of ground truth objects present in the image. Analogously, the set of predictions generated by DETR, parameterized by θ , is denoted by $\hat{\mathcal{T}}_\theta(x)$. Each prediction $t \in \hat{\mathcal{T}}_\theta(x)$ is characterized by a bounding box \hat{b} and an associated class label with a corresponding probability \hat{p} .

The structure of DETR is composed of two main components: the Transformer encoder, which extracts a collection of features from the given image; and the Transformer decoder, which uses these features to make predictions. In addition to the features extracted by the encoder, the decoder’s input consists of M (typically several hundred) learnable embeddings, also known as *object queries*. Each decoder

layer is composed of a self-attention module among object queries and a cross-attention module between each object query and the features. After processing the queries through several decoder layers, the model produces the M final representation vectors that are converted into bounding boxes and class labels via a shared feedforward network, f_ϕ . Together, these predictions form the final outputs, making DETR’s predictions essentially an M -element set. We refer to Figure 4 in the Appendix for an illustration.

The encoder follows the common structure of standard computer vision models and is based on pre-trained models, whose reliability has been relatively widely explored [20, 26, 27, 29]. This foundation further enables the use of prominent post hoc UQ techniques, such as Monte Carlo dropout [7, 29] and distance-based out-of-distribution (OOD) detection methods [4, 12, 28]. However, despite the decoder being the predominant component for object detection, there is a gap in understanding and quantifying its reliability due to its unique structural characteristic: set prediction. Therefore, this paper delves into the underlying characteristics of these predictions and presents a methodology to quantify the reliability of the decoder in DETR for object detection tasks.

2.2. Identifying Reliable Predictions in DETR

Notably, the number of predictions generated by DETR, $|\widetilde{\mathcal{T}}_\theta(\mathbf{x})|$, is fixed and often in the hundreds, far exceeding the number of ground truth objects. To address the issue, during model training, a bipartite matching algorithm is used to find the *optimal* matching prediction for each ground truth object based on the alignment of the class label and bounding box (as detailed in Appendix B). Consequently, the parameters θ are optimized to enhance the accuracy of these matched queries. In this paper, we refer to the matched queries as *optimal positive* queries, while the remaining queries are termed *optimal negative* queries.

At the inference stage in real-world scenarios, however, ground truth annotations are unavailable, meaning the optimal positive queries remain unknown. This raises the question of **whether all predictions can be trusted and used without any post-processing, or if only a subset should be selected for the final inference—and, if so, which subset?** If all of the model’s predictions, including negative queries, were generated independently and were nearly identical to one of the positive predictions, the large number of predictions would not be a concern. We could simply apply well-known algorithms like NMS to remove duplicates and resolve redundancy. Notably, we have observed that DETR assigns well-calibrated confidence scores to only a single positive query (i.e., prediction) per object, while assigning low scores but similar bounding boxes to negative queries (see Section 3.1 and Figure 2). As a result, the overall prediction-level calibration error becomes sig-

nificantly high (See Section 3.2) if we include those noisy predictions in the final inference results. Hence, improper handling of negative queries (e.g., by using top-100 predictions) can severely compromise DETR’s reliability, with potentially catastrophic consequences in safety-critical scenarios, such as pedestrian detection in autonomous vehicles. For this reason, addressing this challenge and effectively distinguishing the positives from negatives is a crucial task for ensuring reliable UQ in DETR.

3. Analysis and Key Insights

3.1. Exploring the Anatomy of DETR’s Predictions

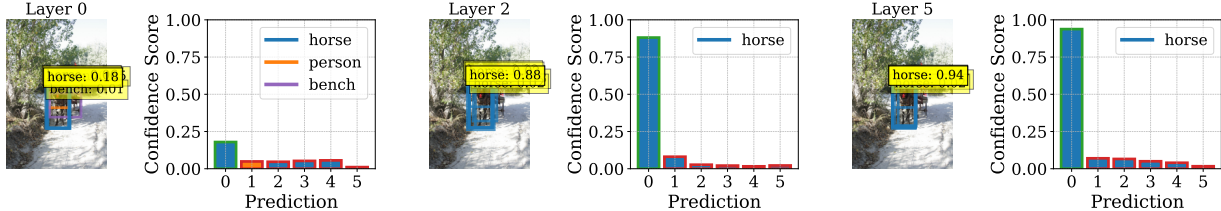
We begin by closely examining the underlying dynamics of DETR decoders and visualizing the generated outputs. Since the Transformer decoder outputs only representation vectors, investigating their evolution across layers is not straightforward. We address this by reapplying the final feedforward network that operates on the last layer, f_ϕ , to the intermediate layers. This allows us to transform each representation vector into its associated bounding box and class label. This is feasible due to the alignment of intermediate representations, facilitated by residual connections between decoder layers [2]. Sample visualizations are in Figure 2 along with Figures 5 and 6 in Appendix C.

In the first decoder layer, the model appears to explore the encoded image features, producing varied queries that result in various plausible predictions. In this early stage, the distinction between positive and negative queries can be ambiguous (e.g., Figure 2a). However, the self-attentions through the subsequent decoder layers progressively refine these predictions. By the final layer, the model selects a single query (i.e., optimal positive) and assigns a confidence score based on its understanding of the image and the object. In contrast, the confidence scores for neighboring queries (i.e., optimal negatives) do not increase to the same extent as the positives and even decrease in high-reliability images. In contrast, in low-reliability images (e.g., Figure 2b), the confidence score of the positive query does not significantly increase, while the scores of the negative ones are either slightly raised or unchanged. Based on this observation, we present our claim:

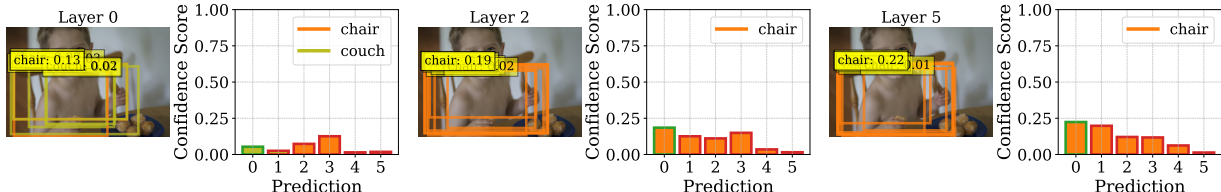
Claim 1. *Predictions from DETR within a given image exhibit varying levels of reliability. For each object in the image, the optimal positive (i.e., best-matched) prediction is calibrated, while the remaining optimal negative predictions are uncalibrated.*

3.2. Analysis of Calibration Error for Positive and Negative Predictions

Primarily, to address the first research question (RQ1) and provide quantitative support for our claim regarding the varying levels of reliability across predictions, we evaluate



(a) A prediction in high-reliability image: Horse



(b) A prediction in low-reliability image: Chair

Figure 2. Visualizations of the predictions generated by Cal-DETR. The optimal positive prediction (indexed by 0 and bordered in green) and the five optimal negative predictions (indexed by 1-5 and bordered in red) with the largest IoU are presented. For each prediction and layer, the maximum confidence score and its corresponding label are visualized. When the model is confident, the confidence score of the positive prediction either increases or remains high across the decoder layers, while those of negative predictions decrease or stay low. On the other hand, when the model is uncertain, DETR assigns a confidence score to positive prediction based on its confidence, thereby maintaining good calibration. However, conversely, it slightly increases or maintains the confidence scores for negative predictions.

and compare the calibration errors on the optimal positive predictions and the optimal negative predictions. The optimal positives and negatives are determined using the standard bipartite matching algorithm [1].

We evaluate the object-level calibration error, which is defined later in Section 4.2. From Table 1, we confirm our claim that *only the optimal positive predictions are properly-calibrated*. Furthermore, as illustrated in Figure 2, the optimal negative predictions exhibit a significantly high calibration error, driven by consistently low confidence scores regardless of their actual accuracy. It is also noteworthy that even Cal-DETR, the state-of-the-art calibrated DETR variant, demonstrates poor calibration quality for optimal negative predictions.

Moreover, as will be explained in more detail later, Table 3 further supports our claim by illustrating that distinguishing between positive and negative predictions becomes particularly crucial when applied to image-level UQ in DETR. In short, when confidence scores are averaged without distinguishing positive queries (see the row of Conf^+ using the top-100 predictions), the correlation between the confidence scores and image-level reliability (i.e., precision) becomes negative. This is because the average confidence scores for negative queries are shown to be *inversely* correlated with image-level reliability, and the majority of DETR’s outputs are actually negative. These results further highlight the importance of employing an appropriate separation scheme to accurately identify optimal positive predictions, even when ground truth annotations

Table 1. Object-level calibration error on top-100, optimal positive, and negative predictions are reported across various models and datasets. For each model, the smallest and largest errors are highlighted in blue and red, respectively. Notably, negative queries are uncalibrated. Since the top-100 predictions often include these negative queries, the resulting calibration error tends to be high.

Model	Predictions	COCO	City	Foggy
D-DETR	Top-100	0.582	0.552	0.618
	Negative	0.803	0.789	0.844
	Positive	0.275	0.341	0.419
UP-DETR	Top-100	0.660	0.689	0.709
	Negative	0.872	0.871	0.883
	Positive	0.438	0.494	0.546
Cal-DETR	Top-100	0.655	0.668	0.688
	Negative	0.867	0.859	0.871
	Positive	0.425	0.463	0.513
DINO	Top-100	0.635	0.693	0.713
	Negative	0.953	0.959	0.962
	Positive	0.411	0.480	0.544

are unavailable.

4. A Systematic Framework for Identifying Positive Predictions

Identifying the positive predictions is crucial for the reliable use of DETR. Nonetheless, identifying optimal positive predictions during the inference stage is not feasible due to the lack of ground truth labels. Therefore, an alternative systematic framework is essential not only for improving its interpretability but also for ensuring reliability. Given that the optimal matching achieves the smallest calibration error, **we use calibration error to measure the quality of a**

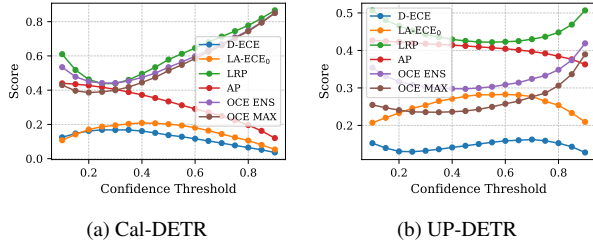


Figure 3. Impact of confidence threshold selection on various performance metrics in Cal-DETR and UP-DETR on COCO.

separation scheme, i.e., a separation scheme with a lower calibration error is deemed a better scheme.

4.1. Limitations of Existing Metrics

To this end, this section analyzes the effectiveness of existing metrics, including AP, D-ECE, LA-ECE₀, and LRP, for measuring calibration error. Specifically, we modify a variable (e.g., the confidence score threshold) to generate different subsets of DETR predictions. We then assess the performance of each metric for these subsets and determine the variable value that yields the highest performance. Lastly, we evaluate the extent of separation by comparing the predicted positive set to the optimal positive set. Sample analysis results are illustrated in Figure 3. For additional results and detailed information on these metrics, please refer to Appendix D.

Primarily, as noted in several studies [11, 18, 19] and our empirical findings, the optimal AP is achieved when the threshold is set to 0.0; AP does not penalize harshly for having low confidence predictions. However, as discussed earlier, using the entire prediction set carries a high risk of including uncalibrated negatives, leading to unreliable decisions in practical applications. Furthermore, using hundreds of predictions harms the interpretability of the model.

In contrast, the optimal ECEs are often achieved when the threshold is set close to 1.0, meaning ECEs favor retaining fewer predictions with high confidence. This is a structural pitfall that prediction-level ECEs commonly face [11]. Since ECEs do not penalize missed detections (i.e., false negatives), they can achieve near-zero error when the evaluation positive set consists solely of highly accurate and confident predictions. Therefore, unless the model is trained to be excessively overconfident—which is unlikely given that DETR is trained on large datasets using various auxiliary loss functions—ECEs can result in very small error values when using a large confidence threshold.

LRP [18], a localization-aware performance metric, can be used instead. However, LRP is not designed as a calibration metric and does not explicitly consider calibration error. As a result, the ranking scored by LRP across the different models is not necessarily aligned with the model’s

calibration qualities. See Section 6.1 for the numerical analysis and more discussions.

4.2. Proposed Metric: Object-Level Calibration Error

Notation. For each image \mathbf{x}_i having N_i objects, we consider the ground truth set $\mathcal{T}_{\mathbf{x}_i} = \{o_{i,j} = (l_{i,j}, \mathbf{b}_{i,j})\}_{j=1}^{N_i bu}$, and a set of DETR predictions: $\hat{\mathcal{T}}_{\theta}(\mathbf{x}_i) = \{t_{i,q} = (\hat{\mathbf{p}}_{i,q}, \hat{\mathbf{b}}_{i,q})\}_{q=1}^M$ where M represents the number of object queries. Here, $l_{i,j} \in [1, C]$ and $\hat{\mathbf{p}}_{i,q} \in \{0, 1\}^C$ represents the ground-truth label and predicted probability distribution over C classes, respectively, while $\mathbf{b}_{i,j}$ and $\hat{\mathbf{b}}_{i,q} \in \{0, 1\}^4$ corresponds to the ground truth and predicted scaled bounding box, respectively.

Definition 1. Consider a subset of predictions, $\hat{\mathcal{S}}_{\theta}(\mathbf{x}_i) \subseteq \hat{\mathcal{T}}_{\theta}(\mathbf{x}_i)$, that is generated by post-processing algorithm \mathcal{S} from the entire prediction set: $\hat{\mathcal{S}}_{\theta} = \mathcal{S} \circ \hat{\mathcal{T}}_{\theta}$. We define an object-level calibration error (OCE) as the average Brier score per object:

$$\text{OCE}(\hat{\mathcal{S}}_{\theta}; \mathcal{I}) \triangleq \frac{1}{|\mathcal{I}|} \sum_{(i,j) \in \mathcal{I}} \text{Brier}(\hat{\mathcal{S}}_{\theta}(\mathbf{x}_i); o_{i,j}) \quad (1)$$

$$\text{Brier}(\hat{\mathcal{S}}_{\theta}(\mathbf{x}_i); o_{i,j}) = \sum_{c=1}^C (\mathbb{1}(c = l_{i,j}) - \tilde{p}_{i,j}[c])^2 \quad (2)$$

$$\tilde{p}_{i,j}[c] = \frac{1}{|\mathcal{Q}_{i,j}|} \sum_{q \in \mathcal{Q}_{i,j}} \hat{\mathbf{p}}_{i,q}[c] \quad (3)$$

where $\mathcal{I} = \cup_i \{(i, j)\}_{j=1}^{N_i}$ is a set of all objects indices and $\hat{\mathbf{p}}(\cdot)[c]$ outputs the probability of c -th class; $\mathcal{Q}_{i,j}$ is a set of query indices that matches to the ground truth object $o_{i,j}$ and we propose two variants:

$$\mathcal{Q}_{i,j} \triangleq \{q \mid \text{IoU}(\mathbf{b}_{i,j}, \hat{\mathbf{b}}_{i,q}) \geq \epsilon\} \quad (\text{OCE}_{\text{ENS}\epsilon}) \quad (4)$$

$$\mathcal{Q}_{i,j} \triangleq \{q = \text{argmin}_q \text{IoU}(\mathbf{b}_{i,j}, \hat{\mathbf{b}}_{i,q})\} \quad (\text{OCE}_{\text{MAX}}) \quad (5)$$

The difference is that $\text{OCE}_{\text{ENS}\epsilon}$ ensembles the overlapping predictions, while OCE_{MAX} selects the prediction with the best bounding-box matching. When $|\mathcal{Q}_{i,j}| = 0$, we consider the predicted probability to be zero, thus the corresponding Brier score is estimated as 1.0. Following [11, 14], we use IoU thresholds of $\epsilon = 0.5, 0.75$ and report the average score as OCE_{ENS} or simply OCE .

The introduced calibration error has two desirable characteristics. First, the prediction set achieves the lowest calibration error when the predictions are well-calibrated to the respective closest ground truth objects. Second, it penalizes the subset, $\hat{\mathcal{S}}_{\theta}(\cdot)$, that includes missing ground truth objects; this ensures that subsets containing a small set of highly precise predictions are not assigned an artificially low error, unlike D-ECE and LA-ECE metrics. Thus, this metric

can effectively assess not only whether the given subsets $\{\hat{\mathcal{S}}_\theta(\mathbf{x}_i)\}_i$ are reliable, but also whether they comprehensively capture all ground truth objects, providing richer information compare to existing metrics.

5. Use-Case Implications

5.1. Image-Level Reliability

As a main use-case implication of this research, this paper investigates how effective separation impacts the performance of quantifying image-level reliability within the DETR framework. Specifically, we first introduce a formal definition of *image-level reliability* by examining the model’s overall object detection performance on the image.

Definition 2. We define image-level reliability as a measure of how accurately and confidently the predictions match the ground truth objects:

$$\text{ImReli}(\mathbf{x}; \theta) \triangleq \text{Perf}(\hat{\mathcal{T}}_\theta(\mathbf{x}), \mathcal{T}_\mathbf{x}). \quad (6)$$

where one can quantify Perf using any standard performance metrics such as average precision, depending on the specification.

By its definition, image-level reliability directly addresses the model’s applicability to a given test instance. However, since image-level reliability requires ground truth annotations for its determination, obtaining it during inference is not feasible. Therefore, our goal is to employ a proxy method that quantifies uncertainty or confidence, which should closely correlate with image-level reliability.

5.2. Proposed Framework: Quantifying Reliability by Contrasting

As illustrated, positive and negative queries exhibit varying levels of reliability. Interestingly, having queries with low confidence scores does not necessarily imply low reliability. Our empirical observations show that confidence scores in negative queries actually *inversely correlate* with image-level reliability. More specifically, for a **reliable** instance, we observe that the confidence of positive queries increases across the decoder layers, while that of negative queries remains low; this results in a **large gap between positive and negative queries**. In contrast, for **unreliable** instances (e.g., Figure 2a), the confidence score of the positive query does not increase across the layers, whereas the scores of negative queries are either slightly elevated or remain unchanged. Consequently, there is a **small gap between positive and negative queries** (e.g., Figure 2b).

Based on the finding, we propose a post hoc UQ approach by contrasting the confidence scores of positives and

negatives:

$$\text{ContrastiveConf}(\mathbf{x}) = \text{Conf}^+(\mathbf{x}) - \lambda \text{Conf}^-(\mathbf{x}) \quad (7)$$

$$\text{Conf}^+(\mathbf{x}) = \frac{1}{|\hat{\mathcal{T}}_\theta^+(\mathbf{x})|} \sum_{t \in \hat{\mathcal{T}}_\theta^+(\mathbf{x})} \mathbf{c}(t) \quad (8)$$

$$\text{Conf}^-(\mathbf{x}) = \frac{1}{|\hat{\mathcal{T}}_\theta^-(\mathbf{x})|} \sum_{t \in \hat{\mathcal{T}}_\theta^-(\mathbf{x})} \mathbf{c}(t) \quad (9)$$

where $\hat{\mathcal{T}}_\theta^+(\mathbf{x})$ and $\hat{\mathcal{T}}_\theta^-(\mathbf{x})$ are predicted sets of positive and negative predictions, respectively, and λ is a scaling factor, that can be selected from the validation set. We include an ablation study of the scaling factor in the supplementary material. Our results show that the proposed method is not too sensitive to the choice of scaling factor and consistently outperforms baselines, with a scaling factor of 10.0 providing adequate performance. $\mathbf{c}(\cdot)$ denotes the confidence estimate for the prediction; in this paper, we use maximum probability, $\mathbf{c}(t = (\hat{\mathbf{p}}, \hat{\mathbf{b}})) = \max_c \hat{\mathbf{p}}[c]$.

As shown so far, identifying a $\hat{\mathcal{T}}_\theta^+(\mathbf{x})$ from $\hat{\mathcal{T}}_\theta(\mathbf{x})$ is a crucial factor in the success of this approach. In practice, however, neither the ground truth (i.e., the queries that DETR intends to use) nor the optimal positives are available during the UQ stage. Instead, we approximate the ground truth separation by applying a post-processing algorithm that minimizes the calibration error on the validation set:

$$\hat{\mathcal{T}}_\theta^+(\mathbf{x}) = \mathcal{S}^* \circ \hat{\mathcal{T}}_\theta(\mathbf{x}) \quad (10)$$

$$\mathcal{S}^* = \operatorname{argmin}_{\mathcal{S}} \text{OCE}(\mathcal{S} \circ \hat{\mathcal{T}}_\theta; \mathcal{I}_{\text{val}}) \quad (11)$$

where $\mathcal{I}_{\text{val}} = \cup_{i \in \mathcal{V}} \{(i, j)\}_{j=1}^{O_i}$ is the set of all objects indices in the validation dataset \mathcal{V} . Unless specified otherwise, we adopt confidence thresholding for the separation scheme (i.e., post-processing algorithm), where the corresponding threshold is the variable to optimize.

6. Experiments

To demonstrate the effectiveness of the proposed method, we conducted experiments using four DETR variants: UP-DETR [3], Deformable-DETR (D-DETR), Cal-DETR [17], and DINO. Each model is trained on the COCO (train2017) dataset and we use 1,000 images (i.e., 20%) of COCO (val2017) for the validation set and the remaining images for the test set. The model is tested on three datasets with varying levels of out-of-distribution (OOD) characteristics: COCO (in-distribution), Cityscapes (near OOD), and Foggy Cityscapes (OOD). Experimental details can be found in Appendix E.

6.1. Effectiveness of OCE

To showcase OCE’s effectiveness in assessing calibration quality, we analyze how different metrics rank calibration

Table 2. Comparison of the effectiveness of the proposed OCE and baseline metrics, focusing on their ranking correlation with the rankings given by the models’ calibration quality on optimal positive predictions (denoted by the superscript *). For each metric, various post-processing schemes (i.e., ways to identify positive predictions) are applied and indicated within parentheses. Correlations exceeding 0.9 are highlighted in blue, while negative correlations are highlighted in red. Our OCE-based rankings consistently provide strong correlations with optimal ranking and OCE effectively measures the model’s calibration quality alongside the post-processing scheme employed.

Methods	COCO (in-distribution)			Cityscapes (near OOD)			Foggy Cityscapes (OOD)			Average	
	D-ECE*	LA-ECE ₀ *	OCE*	D-ECE*	LA-ECE ₀ *	OCE*	D-ECE*	LA-ECE ₀ *	OCE*		
References	D-ECE*	1.000	0.995	0.969	1.000	0.996	0.993	1.000	0.873	0.996	0.980
	LA-ECE ₀ *	0.995	1.000	0.948	0.996	1.000	0.990	0.873	1.000	0.836	0.960
	OCE _{ENS} *	0.969	0.948	1.000	0.993	0.990	1.000	0.996	0.836	1.000	0.970
Baselines	AP (Top-100) [6, 14]	0.552	0.583	0.343	0.779	0.784	0.700	0.597	0.843	0.523	0.634
	LRP (LRP) [18]	0.103	0.051	0.338	-0.268	-0.272	-0.150	-0.257	-0.610	-0.170	-0.137
	D-ECE (Top-100)	-0.873	-0.833	-0.966	0.608	0.576	0.511	-0.254	0.250	-0.316	-0.144
	D-ECE (0.3) [10]	0.905	0.939	0.827	0.982	0.967	0.990	0.964	0.799	0.981	0.928
	D-ECE (LRP)	0.802	0.855	0.659	0.987	0.984	0.999	0.983	0.793	0.996	0.895
	D-ECE (OCE _{ENS})	0.856	0.901	0.727	0.987	0.983	0.999	0.983	0.793	0.996	0.914
	LA-ECE ₀ (Top-100)	-0.944	-0.913	-0.994	-0.431	-0.482	-0.517	-0.786	-0.386	-0.822	-0.697
	LA-ECE ₀ (0.3)	-0.789	-0.729	-0.842	-0.780	-0.818	-0.830	-0.451	-0.041	-0.468	-0.639
	LA-ECE ₀ (LRP) [11]	-0.908	-0.864	-0.948	-0.833	-0.877	-0.846	-0.901	-0.597	-0.913	-0.854
Ours	OCE _{ENS} (OCE _{ENS})	0.962	0.940	1.000	0.987	0.983	0.999	0.964	0.737	0.984	0.951
	OCE _{MAX} (OCE _{MAX})	0.954	0.929	0.998	0.954	0.958	0.983	0.955	0.697	0.976	0.934

error across four DETR models. As baselines, we measure ECEs using the top-100 detections (best AP), a standard confidence threshold of 0.3, and the threshold that minimizes LRP on the validation set. In a similar manner, we assess our OCEs using thresholds that minimize each OCE metric on the validation set. For fair comparison, we execute the optimal matching process on each test dataset to obtain the optimal positive set. We then evaluate D-ECE, LA-ECE₀, and OCE using these sets as reference scores and calculate the Pearson correlation coefficient to the other scoring schemes across different datasets.

As shown in Table 2, our OCE metrics maintain a strong correlation with the optimal ECE metrics across different datasets. This evidence supports the reliability of our OCEs in ranking models by their overall calibration quality on positive sets—which downstream applications are more likely to utilize instead of the top 100 predictions. Notably, LA-ECE₀ with a non-optimal positive set shows an inverse correlation with the rankings estimated on the optimal positive set. Meanwhile, from a model ranking perspective, empirical evidence suggests that solely adopting LRP does not align with calibration qualities. Nonetheless, the ranking by D-ECE and OCE scores measured at the optimal LRP threshold — denoted by D-ECE (LRP) and OCE (LRP), respectively — show a strong correlation to those ranked from the optimal positive set; thus, the method of using LRP to identify a positive set [11] appears acceptable. Experimentally, we confirmed that OCE and LRP provide thresholds in a similar range across different settings.

Another important attribute of OCE is that it can not only be used to compare different models but is also capable of identifying the most reliable configuration of the same model. As illustrated in Figure 3, the confidence vs. OCE

curve exhibits a bell shape, unlike ECE metrics, and the optimal OCE is achieved around a threshold of 0.3. This is particularly notable because it reflects the practical choices in many calibration studies to date [11, 17], affirming the reliability of using OCE.

Using a fixed separation threshold of 0.3 is often a good approximation for distinguishing between optimal positives and negatives (See further discussion in Appendix G). However, trained or post-calibrated DETR models may have varying optimal confidence thresholds (for example, low-temperature calibrated models are likely to have higher optimal thresholds). Therefore, using a fixed threshold can pose a potential risk.

The biggest advantage of using OCE over other metrics is that **OCE measures the model’s calibration quality alongside the post-processing scheme employed**. While measuring the calibration error on the optimal positive set would ideally assess quality, this optimal set is not accessible during test-time inference. Consequently, the score measured on the optimal set may not correspond to the quality experienced in real-world applications, such as those employing confidence thresholding schemes.

6.2. Quantifying Image-Level Reliability

To address the third research question (RQ3), we compare different methods for quantifying per-image reliability using different separation techniques. We measure the Pearson correlation coefficient (PCC) of each method with the ImReli computed based on AP metrics. Additionally, we evaluate the proposed contrasting approach against methods that utilize only positive or negative queries. Empirical results are presented in Table 3 and further in Appendix F. The key takeaways are as follows:

First, as demonstrated throughout our analysis, distin-

Table 3. Comparison of the proposed method (ContrastiveConf) with baseline methods on their Pearson correlation coefficient with the image-level reliability in Equation (6), with different models. Perf is evaluated using AP (Average Precision)[14]. For each model, we apply the optimal matching, the standard post-processing scheme (Top-100 and confidence thresholding by 0.3), and the proposed OCE-based post-processing scheme, as indicated within the parentheses. The strongest correlations are highlighted in bold, while negative correlations appear in red. First, the proposed method achieves the highest correlation with image-level reliability. In addition, it is noteworthy that the average confidence of negative predictions (Conf^-) exhibits a negative correlation with image-level reliability, in contrast to the positive correlation observed when using positive predictions (Conf^+).

Methods	COCO (in-distribution)				Cityscapes (near OOD)				Foggy Cityscapes (OOD)				
	UP-DETR	D-DETR	Cal-DETR	DINO	UP-DETR	D-DETR	Cal-DETR	DINO	UP-DETR	D-DETR	Cal-DETR	DINO	
Oracles	Conf ⁺ (Optimal)	0.503	0.618	0.670	0.635	0.555	0.647	0.649	0.633	0.561	0.642	0.662	0.634
	Conf ⁻ (Optimal)	-0.608	-0.584	-0.572	-0.586	-0.293	-0.296	-0.330	-0.311	-0.177	-0.235	-0.212	-0.196
	ContrastiveConf (Optimal)	0.700	0.684	0.709	0.695	0.601	0.633	0.662	0.634	0.612	0.657	0.672	0.643
Baselines	Conf ⁺ (Top-100)	-0.619	-0.603	-0.581	-0.601	-0.409	-0.374	-0.372	-0.391	-0.262	-0.270	-0.239	-0.229
	Conf ⁺ (0.3)	0.476	0.464	0.539	0.504	0.229	0.353	0.385	0.399	0.195	0.256	0.258	0.258
Ours	Conf ⁺ (OCE)	0.442	0.477	0.547	0.512	0.237	0.355	0.393	0.370	0.228	0.291	0.270	0.274
	Conf ⁻ (OCE)	-0.633	-0.581	-0.571	-0.585	-0.365	-0.389	-0.379	-0.394	-0.245	-0.325	-0.253	-0.283
	ContrastiveConf (OCE)	0.585	0.570	0.597	0.587	0.334	0.432	0.431	0.438	0.287	0.362	0.302	0.327

Table 4. Comparison of different post-processing schemes on OCE (lower is better) and PCC (higher is better) between ContrastiveConf and image-level reliability in Cal-DETR. The thresholding approach consistently yields the best performance.

Schemes	coco		City		Foggy	
	OCE	PCC	OCE	PCC	OCE	PCC
Optimal	0.425	0.695	0.463	0.634	0.513	0.643
Thr	0.454	0.594	0.448	0.464	0.482	0.325
Top- k	0.502	0.527	0.453	0.411	0.492	0.298
NMS	0.555	0.574	0.582	0.373	0.598	0.239

guishing between positive and negative queries is crucial for uncertainty quantification in DETR. Specifically, when confidence scores are averaged without distinguishing positive queries (i.e., Conf^+ w/ top-100), the correlation becomes negative. This occurs because the majority of DETR’s predictions are actually negative (i.e., $|\mathcal{T}_x| \ll |\hat{\mathcal{T}}_\theta(x)|$), and that confidence scores for negative queries are inversely correlated with ImReli .

Second, the proposed ContrastiveConf consistently achieves the best correlation with image-level reliability. Interestingly, the absolute value of Conf^- occasionally outperforms ContrastiveConf when a non-optimal separation scheme is applied; however, its performance varies across different settings. This variability underscores the robustness of our contrasting approach, which leverages the strengths of both Conf^+ and Conf^- .

6.3. Comparative Study on Post-Processing

Lastly, we present a comparative analysis across different post-processing schemes for identifying positive queries in DETR, from the reliability perspective. We assess OCE for each predicted positive to evaluate the impact of various separation schemes on calibration performance.

For the separation methods, we compare the following

approaches: (1) applying a **threshold** on the confidence score, (2) selecting the **top- k** predictions, and (3) utilizing **NMS**. For each method, we evaluate OCE by varying the hyperparameter (e.g., confidence threshold, k , and IoU threshold, respectively) and compare with the score on the **optimal** positive. Likewise, we assess the correlation to image-level reliability for each separation scheme. For each scheme, the best hyperparameter is chosen using the validation set. A summary of the results is provided in Table 4, with the comprehensive results available in Appendix G.

The thresholding approach achieves the smallest OCE and the best image-level UQ performance. In addition, the resulting OCE and correlation is the most comparable to the optimal score, especially for the in-distribution test dataset. The top- k approach underperforms because the number of objects in an image varies significantly, making it impractical to determine a single optimal value for k . The best k ranges from 10 to 20, corresponding to the average number of objects per image in the COCO dataset. On the other hand, with NMS (when applied without preceding confidence thresholding), we empirically observe that although most of the optimal positive queries are included, a substantial number of negative queries are retained, often outnumbering the positive ones by several times. Nonetheless, a performance gap remains compared to optimal matching, especially on out-of-distribution datasets. Addressing this gap is left for future work.

7. Conclusion and Limitations

The main contribution of our work is an in-depth analysis of the importance of post-processing in DETR frameworks. Furthermore, this paper demonstrates the impact of the post-separation method on the reliability of their predictions, and proposes a novel UQ method for quantifying image-level reliability in DETR.

The primary limitation of our work is that our analysis is

confined to standard separation schemes, such as thresholding, without proposing a novel separation technique. We conjecture that leveraging information from intermediate layers, rather than solely relying on final predictions, can achieve more robust separation because positive and negative queries follow different evolutionary patterns. One potential approach is to enable the model to explicitly output matching probabilities by introducing an auxiliary loss during training, as proposed by Oksuz et al. [19].

Acknowledgments

The authors acknowledge the MIT SuperCloud and Lincoln Laboratory Supercomputing Center for providing computing resources that have contributed to the results reported within this paper. This work was supported in part by the MIT Summer Research Program (MSRP), the MIT-Google Program for Computing Innovation, the MIT-Amazon Science Hub, the MIT-IBM Watson AI Lab, and MathWorks.

References

- [1] Nicolas Carion, Francisco Massa, Gabriel Synnaeve, Nicolas Usunier, Alexander Kirillov, and Sergey Zagoruyko. End-to-end object detection with transformers. In *European conference on computer vision*, pages 213–229. Springer, 2020. [1](#), [4](#), [12](#)
- [2] Yung-Sung Chuang, Yujia Xie, Hongyin Luo, Yoon Kim, James Glass, and Pengcheng He. Dola: Decoding by contrasting layers improves factuality in large language models. *arXiv preprint arXiv:2309.03883*, 2023. [3](#)
- [3] Zhigang Dai, Bolun Cai, Yugeng Lin, and Junying Chen. Up-detr: Unsupervised pre-training for object detection with transformers. In *Proceedings of the IEEE/CVF conference on computer vision and pattern recognition*, pages 1601–1610, 2021. [6](#)
- [4] Xuefeng Du, Gabriel Gozum, Yifei Ming, and Yixuan Li. Siren: Shaping representations for detecting out-of-distribution objects. *Advances in Neural Information Processing Systems*, 35:20434–20449, 2022. [3](#), [11](#)
- [5] Xuefeng Du, Zhaoning Wang, Mu Cai, and Yixuan Li. Vos: Learning what you don’t know by virtual outlier synthesis. *arXiv preprint arXiv:2202.01197*, 2022. [11](#)
- [6] Mark Everingham, Luc Van Gool, Christopher KI Williams, John Winn, and Andrew Zisserman. The pascal visual object classes (voc) challenge. *International journal of computer vision*, 88:303–338, 2010. [2](#), [7](#), [13](#), [15](#)
- [7] Yarin Gal and Zoubin Ghahramani. Dropout as a bayesian approximation: Representing model uncertainty in deep learning. In *international conference on machine learning*, pages 1050–1059. PMLR, 2016. [3](#), [11](#)
- [8] Ross Girshick, Jeff Donahue, Trevor Darrell, and Jitendra Malik. Rich feature hierarchies for accurate object detection and semantic segmentation. In *Proceedings of the IEEE conference on computer vision and pattern recognition*, pages 580–587, 2014. [1](#)
- [9] Kaiming He, Georgia Gkioxari, Piotr Dollár, and Ross Girshick. Mask r-cnn. In *Proceedings of the IEEE international conference on computer vision*, pages 2961–2969, 2017. [1](#)
- [10] Fabian Kuppers, Jan Kronenberger, Amirsossein Shantia, and Anselm Haselhoff. Multivariate confidence calibration for object detection. In *Proceedings of the IEEE/CVF conference on computer vision and pattern recognition workshops*, pages 326–327, 2020. [1](#), [2](#), [7](#), [11](#), [12](#), [15](#)
- [11] Selim Kuzucu, Kemal Oksuz, Jonathan Sadeghi, and Puneet K Dokania. On calibration of object detectors: Pitfalls, evaluation and baselines. In *European Conference on Computer Vision*, pages 185–204. Springer, 2025. [2](#), [5](#), [7](#), [12](#), [15](#)
- [12] Kimin Lee, Kibok Lee, Honglak Lee, and Jinwoo Shin. A simple unified framework for detecting out-of-distribution samples and adversarial attacks. *Advances in neural information processing systems*, 31, 2018. [3](#)
- [13] Ruoqi Li, Chongyang Zhang, Hao Zhou, Chao Shi, and Yan Luo. Out-of-distribution identification: Let detector tell which i am not sure. In *European Conference on Computer Vision*, pages 638–654. Springer, 2022. [11](#)
- [14] Tsung-Yi Lin, Michael Maire, Serge Belongie, James Hays, Pietro Perona, Deva Ramanan, Piotr Dollár, and C Lawrence Zitnick. Microsoft coco: Common objects in context. In *Computer Vision–ECCV 2014: 13th European Conference, Zurich, Switzerland, September 6–12, 2014, Proceedings, Part V 13*, pages 740–755. Springer, 2014. [2](#), [5](#), [7](#), [8](#), [13](#), [15](#)
- [15] Muhammad Akhtar Munir, Muhammad Haris Khan, M Sarfraz, and Mohsen Ali. Towards improving calibration in object detection under domain shift. *Advances in Neural Information Processing Systems*, 35:38706–38718, 2022. [1](#)
- [16] Muhammad Akhtar Munir, Muhammad Haris Khan, Salman Khan, and Fahad Shahbaz Khan. Bridging precision and confidence: A train-time loss for calibrating object detection. In *Proceedings of the IEEE/CVF Conference on Computer Vision and Pattern Recognition*, pages 11474–11483, 2023.
- [17] Muhammad Akhtar Munir, Salman H Khan, Muhammad Haris Khan, Mohsen Ali, and Fahad Shahbaz Khan. Cal-detr: calibrated detection transformer. *Advances in neural information processing systems*, 36, 2024. [1](#), [6](#), [7](#)
- [18] Kemal Oksuz, Baris Can Cam, Emre Akbas, and Sinan Kalkan. Localization recall precision (lrp): A new performance metric for object detection. In *Proceedings of the European conference on computer vision (ECCV)*, pages 504–519, 2018. [5](#), [7](#), [11](#), [13](#), [15](#)
- [19] Kemal Oksuz, Tom Joy, and Puneet K Dokania. Towards building self-aware object detectors via reliable uncertainty quantification and calibration. In *Proceedings of the IEEE/CVF Conference on Computer Vision and Pattern Recognition*, pages 9263–9274, 2023. [2](#), [5](#), [9](#), [11](#), [12](#)
- [20] Young-Jin Park, Hao Wang, Shervin Ardestir, and Navid Azizan. Quantifying representation reliability in self-supervised learning models. *arXiv preprint arXiv:2306.00206*, 2023. [3](#)
- [21] Bimsara Pathiraja, Malitha Gunawardhana, and Muhammad Haris Khan. Multiclass confidence and localization calibration for object detection. In *Proceedings of the IEEE/CVF*

Conference on Computer Vision and Pattern Recognition, pages 19734–19743, 2023. 1

- [22] Joseph Redmon, Santosh Divvala, Ross Girshick, and Ali Farhadi. You only look once: Unified, real-time object detection. In *Proceedings of the IEEE conference on computer vision and pattern recognition*, pages 779–788, 2016. 1
- [23] Shaoqing Ren, Kaiming He, Ross Girshick, and Jian Sun. Faster r-cnn: Towards real-time object detection with region proposal networks. *Advances in neural information processing systems*, 28, 2015. 1
- [24] Hamid Rezatofighi, Nathan Tsoi, Jun Young Gwak, Amir Sadeghian, Ian Reid, and Silvio Savarese. Generalized intersection over union: A metric and a loss for bounding box regression. In *Proceedings of the IEEE/CVF conference on computer vision and pattern recognition*, pages 658–666, 2019. 12
- [25] Gerard Salton. Introduction to modern information retrieval. *McGrawHill Book Co*, 1983. 2
- [26] Apoorva Sharma, Navid Azizan, and Marco Pavone. Sketching curvature for efficient out-of-distribution detection for deep neural networks. In *Uncertainty in artificial intelligence*, pages 1958–1967. PMLR, 2021. 3
- [27] Artem Shelmanov, Evgenii Tsymbalov, Dmitri Puzyrev, Kirill Fedyanin, Alexander Panchenko, and Maxim Panov. How certain is your transformer? In *Proceedings of the 16th Conference of the European Chapter of the Association for Computational Linguistics: Main Volume*, pages 1833–1840, 2021. 3, 11
- [28] Jihoon Tack, Sangwoo Mo, Jongheon Jeong, and Jinwoo Shin. CSI: Novelty detection via contrastive learning on distributionally shifted instances. *Advances in neural information processing systems*, 33:11839–11852, 2020. 3
- [29] Artem Vazhentsev, Gleb Kuzmin, Artem Shelmanov, Akim Tsvigun, Evgenii Tsymbalov, Kirill Fedyanin, Maxim Panov, Alexander Panchenko, Gleb Gusev, Mikhail Burtsev, et al. Uncertainty estimation of transformer predictions for misclassification detection. In *Proceedings of the 60th Annual Meeting of the Association for Computational Linguistics (Volume 1: Long Papers)*, pages 8237–8252, 2022. 3, 11
- [30] Samuel Wilson, Tobias Fischer, Feras Dayoub, Dimity Miller, and Niko Sünderhauf. Safe: Sensitivity-aware features for out-of-distribution object detection. In *Proceedings of the IEEE/CVF International Conference on Computer Vision*, pages 23565–23576, 2023. 11
- [31] Hao Zhang, Feng Li, Shilong Liu, Lei Zhang, Hang Su, Jun Zhu, Lionel M Ni, and Heung-Yeung Shum. Dino: Detr with improved denoising anchor boxes for end-to-end object detection. *arXiv preprint arXiv:2203.03605*, 2022. 1
- [32] Xizhou Zhu, Weijie Su, Lewei Lu, Bin Li, Xiaogang Wang, and Jifeng Dai. Deformable detr: Deformable transformers for end-to-end object detection. *arXiv preprint arXiv:2010.04159*, 2020. 1

A. Related Work

Uncertainty Quantification. Shelmanov et al. [27] and Vazhentsev et al. [29] focus on uncertainty quantification in general Transformer architectures, building upon the MC dropout approach proposed by Gal and Ghahramani [7]. Specifically, they apply a modified MC dropout that prioritizes sample diversity over randomness to improve sample efficiency. However, these methods are not directly applicable to object detection problems because, unlike classification tasks, object detection involves predicting an unordered set. Consequently, it is questionable whether applying MC dropout to each output is appropriate, as the permutation of predictions could be completely shuffled after applying MC dropout.

Several studies focus on out-of-distribution (OOD) identification in object detection models. For example, Li et al. [13] propose a built-in OOD detector to isolate OOD data for human review. This approach can determine OOD scenarios involving both unknown and uncertain classes (i.e., epistemic but not aleatoric uncertainty) by modeling the distribution of training data and assessing whether samples belong to any of the training class distributions. Du et al. [5] generate outlier data from class-conditional distribution estimations derived from in-distribution data, training the model to assign high OOD scores to this generated data and low OOD scores to the original in-distribution data. Similarly, Oksuz et al. [19] employ an auxiliary detection model capable of expressing its confidence. Other works, including Du et al. [4] and Wilson et al. [30], investigate the latent representations generated by object detection models to identify the OOD nature of the input.

To the best of our knowledge, the aforementioned existing uncertainty quantification techniques primarily focus on prediction-level analysis. Moreover, they predominantly address CNN-based models and explore the methodological way to better quantify the uncertainty in object detection model. In contrast, our paper emphasizes the significance of identifying reliable sets within the entire set of predictions for uncertainty quantification, particularly in DETRs. Another novelty of our work lies in investigating an appropriate methodology to integrate different predictions' confidence estimates to quantify image-level reliability.

Calibration. Previous studies primarily addressed OOD detection to assess the prediction-level trustworthiness of DETR. They aim to introduce a framework that does not rely on the model's confidence scores, which can be either overconfident or underconfident, especially for OOD data points. Simultaneously, additional research endeavors to determine the model's overall reliability in its confidence scores. More specifically, these studies assess whether the model's confidence scores align with their actual accuracy.

In other words, low-confidence samples should exhibit low accuracy, and high-confidence samples should demonstrate high accuracy. To evaluate this alignment, they measure the Expected Calibration Error (ECE) by binning predictions based on their confidence scores and computing the mean absolute error between the average confidence and the corresponding accuracy within each bin. However, in object detection tasks, measuring accuracy is not straightforward because predictions comprise both class probabilities and bounding boxes. Additionally, due to the set prediction nature of object detection models, it is unclear which ground truth object corresponds to each prediction. To address these challenges, D-ECE [10] defines precision as the accuracy metric and matches each prediction to a ground truth object based on an IoU threshold (commonly set at 0.5 or 0.75). On the other hand, LaECE [18] defines accuracy as the product of precision and IoU, thereby accounting for localization errors as well.

However, as demonstrated throughout our paper, DETR exhibits poor calibration on optimal negative predictions, while in practice, users prefer to utilize only predicted positive samples (e.g., high-confidence predictions). Therefore, if we rank the model's calibration quality based on the entire prediction set, these rankings are highly biased and thus unreliable. To avoid this issue, previous studies have often measured D-ECE only on predictions with confidence scores exceeding 0.3. As detailed in Appendix G, a threshold of 0.3 approximates the optimal positive predictions in many DETR variants; thus, using such a fixed threshold may be practically acceptable. However, this threshold is not guaranteed to be 0.3 for other models like UP-DETR, which introduces potential risks. In response, our paper addresses the importance of identifying a reliable subset of predictions and proposes the Object-level Calibration Error (OCE) metric, which measures the model's calibration quality alongside the employed post-processing scheme and thus can adaptively identify the reliable subset.

Broad Implications. The primary objective of this study is to determine how DETR can be used in a trustworthy manner on new downstream images/tasks and to establish how their predictions should be properly used, which has several important implications. For example, when building an auto-labeling system using data-driven detection models like DETR, it is crucial to consider that the model may not always provide accurate predictions. As a result, when the model's reliability for a specific image is in question, the image might need to be reviewed by a human labeler. Therefore, evaluating reliability at the image level is often necessary to assess the model's overall understanding of the given test image. Furthermore, by providing a comprehensive analysis for identifying a reliable subset of predictions, our study offers users a systematic and trustworthy method

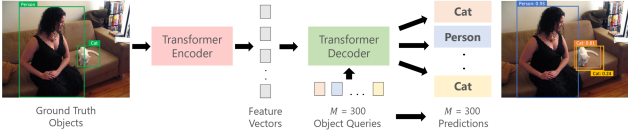


Figure 4. A diagram of the DETR architecture. An input image is first processed through a CNN backbone to generate a 2D feature representation. This representation is then passed to the Transformer encoder, which extracts feature vectors. These feature vectors are sent to the decoder, which receives M learned object queries together. The decoder outputs M prediction sets, each containing a bounding box and corresponding class probabilities. Please refer to the original papers for details.

for post-processing the outputs of DETR. We hope our efforts expand the scope of DETR applications by enabling more precise and reliable deployment, sparking further research into the area of positive prediction identification.

B. Bipartite Matching: Positive & Negative Queries

Since the number of queries in DETR, M , is much higher than the number of ground truth objects, DETR matches each ground truth object with the corresponding best model prediction during its training. To compute this optimal (i.e., ground truth) matching for the predictions in a given image, a bipartite matching algorithm is applied. More specifically, a matching cost between each pair of a given prediction and a ground truth object is defined as follows:

$$\mathcal{L}_{\text{matching}} = \mathcal{L}_{\text{class}} + \mathcal{L}_{\text{box}} \quad (12)$$

where $\mathcal{L}_{\text{class}}$ is the negative prediction confidence of the ground truth class and \mathcal{L}_{box} is the linear combination of the ℓ_1 loss between the corners of the bounding boxes and \mathcal{L}_{iou} . \mathcal{L}_{iou} is the Generalized Intersection over Union (GIoU) [24] loss between bounding boxes. After computing this matching cost for every combination of prediction set and ground truth objects, DETR then efficiently calculates the permutation that minimizes the total matching cost using the Hungarian matching algorithm.

In this paper, we then refer to those matched queries as positive predictions and the remaining unmatched queries as negative predictions. More details on the bipartite matching process and Hungarian algorithm can be found in [1].

C. Further Visualizations of How DETR Generates Predictions

The predictions across all six decoder layers for each of the images presented in the main paper are provided in Figure 5. Another noticeable example is provided in Figure 6, where

predictions for two different objects, a dog and a laptop, are shown for the same low-reliability image. In Figure 6a, for the laptop object, all of the queries start off with low confidence and remain that way over the course of the layers. However, the class predictions gradually shift from dining table and person to laptop, and result in an overall low confidence score despite a correct final prediction (laptop).

However, Figure 6b indicates that even in a low-reliability image there can still be reliable predictions. For the dog object, the model is very confident in its predictions from the start, with many overlapping prediction sets in the same area and with matching classes. While there are two dominant predictions in the first layer, DETR focuses on a single prediction (query 0) while the confidence for query 1 is gradually reduced; this aligns with the trend observed in the reliable examples shown earlier.

D. Performance Metrics

D.1. Expected Calibration Error (ECE) Metrics

Detection Expected Calibration Error (D-ECE) [10] is a calibration metric that specifically focuses on calibrating the confidence of an object detection model to align with precision. The confidence space is divided into J bins, and then D-ECE is computed as follows:

$$\text{D-ECE} \triangleq \sum_{j=1}^J \frac{|\hat{\mathcal{D}}_j|}{|\hat{\mathcal{D}}|} |\bar{p}_j - \text{precision}(j)| \quad (13)$$

where $\hat{\mathcal{D}}$ and $\hat{\mathcal{D}}_j$ are the set of all detections and the detections in the j -th bin, and \bar{p}_j and $\text{precision}(j)$ are the average confidence and the precision of the detections in the j -th bin. D-ECE identifies true positive (TP) samples by confirming the accuracy of class labels and ensuring that the IoU surpasses the threshold τ . Following the standard protocol [11], this work measures D-ECE using thresholds $\tau = 0.5$ and $\tau = 0.75$, and then averages the scores.

To account for both localization error and classification precision, LaECE [11, 19] calibrates model confidence to the product of precision and the IoU between the bounding box predictions and ground-truth boxes. LaECE is computed in a class-wise manner to combat class imbalance, as follows:

$$\text{LaECE} \triangleq \frac{1}{K} \sum_{c=1}^K \sum_{j=1}^J \frac{|\hat{\mathcal{D}}_j^c|}{|\hat{\mathcal{D}}^c|} |\bar{p}_j^c - \text{precision}^c(j) \times \text{IoU}^c(j)| \quad (14)$$

where c refers to each class and $\text{IoU}^c(j)$ refers to the average IoU of $\hat{\mathcal{D}}_j^c$. Similar to D-ECE, LaECE requires an IoU threshold, τ . In contrast, LaECE₀ proposes to set this threshold τ to 0 and instead set $\text{IoU}^c(\cdot) = 0$ for the false

positive (FP) samples. This leads to a reduction of the calibration criterion of LaECE as follows:

$$\text{LaECE}_0 = \frac{1}{K} \sum_{c=1}^K \sum_{j=1}^J \frac{|\hat{\mathcal{D}}_j^c|}{|\hat{\mathcal{D}}^c|} |\bar{p}_j^c - \text{IoU}^c(j)| \quad (15)$$

D.2. Performance Metrics

Average precision (AP) [6] is the most common accuracy metric for object detectors. Before calculating AP, the top- k (e.g., typically 100) class predictions for a given image are kept and sorted, while the others are discarded. Then, in order of this sorting, the predictions are compared against the ground-truth bounding boxes, and the predicted label is compared with the ground truth label if the IoU is large enough. The precision/recall curve is calculated over the sorted predictions, and AP averages the precision across a set of 101 evenly spaced recall thresholds:

$$\text{AP} = \frac{1}{101} \sum_{r \in [0:0.01:1]} p(r) \quad (16)$$

where $p(r)$ is calculated by the maximum precision at recall level r .

Localization recall precision (LRP) [18] considers the number of true positives, false positives, and false negatives with localization error, represented by N_{TP} , N_{FP} , and N_{FN} , respectively:

$$\text{LRP}_\tau = \frac{1}{N_{\text{FP}} + N_{\text{FN}} + N_{\text{TP}}} \left(N_{\text{TP}} + N_{\text{FN}} + \sum_{i=1}^{N_{\text{TP}}} \frac{1 - \text{IoU}_i}{1 - \tau} \right) \quad (17)$$

where τ is IoU threshold, i denotes the index of each true positive prediction, and IoU_i represents the IoU between that prediction and the best-matching ground-truth object. LRP is then computed by averaging $\text{LRP}_{0.5}$ and $\text{LRP}_{0.75}$.

D.3. Impact of Separation Schemes on Metrics

The trends presented in Figure 3 also hold for other datasets and models. Figure 7 shows the performance of the model according to different metrics with various confidence thresholds (i.e. post-processing schemes). As illustrated in Section 4.1, the optimal AP is achieved when the threshold is set to 0.0. In contrast, the optimal ECEs are often achieved when the threshold is set close to 1.0, meaning ECEs favor retaining fewer predictions with high confidence. However, as discussed earlier, using the entire or small subset carries a high risk of including uncalibrated negatives or having missing detections, leading to unreliable decisions in practical applications and diminished interpretability.

E. Experiment Setup

For our experiments, we used the Cityscapes and Foggy Cityscapes datasets, which each have 500 images of first-person driving footage in realistic environments. Foggy Cityscapes has the same base images as Cityscapes, but with fog simulated and added to create a further out of distribution set. Since the DETR models were trained on COCO, the Cityscapes and Foggy Cityscapes annotations were converted to correspond to the labels of COCO. More specifically, the person, bicycle, car, motorcycle, bus, train, and truck classes were transferred directly. In addition, the rider class of Cityscapes and Foggy Cityscapes was mapped to the person class of COCO. The other classes present in Cityscapes and Foggy Cityscapes are largely focused on image segmentation, and thus were omitted (e.g. building, sky, sidewalk). The pre-trained model weights were obtained from their respective official implementations.

To compute ImReli for each image, we use the same COCO evaluator [14] to obtain image-wise AP scores. However, rather than passing in the entire image set, the predictions for each image are passed in individually.

F. Further Experimental Results

F.1. Effectiveness of OCE

Table 5 presents the correlations between the rankings provided by three different calibration metrics on the optimal positive set and various methods. The first three rows demonstrate that the calibration metrics—D-ECE, LA-ECE, and our proposed OCE—are highly correlated. This indicates that all three metrics effectively capture the notion of calibration quality. Additionally, these metrics show a decent correlation with AP metrics. It is important to note that AP primarily accounts for accuracy rather than calibration quality, which may explain why the correlation, particularly for AP@50 on the out-of-distribution dataset, is not perfectly aligned.

Furthermore, LRP, D-ECE, and LA-ECE₀ exhibit negative correlations with calibration quality when used alone. This supports our assertion that these metrics are inadequate for measuring models' calibration quality in conjunction with the employed post-processing scheme, unlike our OCE.

Finally, D-ECE exhibits a high correlation when paired with either a fixed threshold or a proper adaptive threshold (i.e., using LRP and our OCE). This is because DETR's optimal positive threshold is empirically found to be around 0.3 (See Table 7.). Consequently, OCE aligns well with the experimentally approximated threshold and the LRP metric in identifying effective post-processing schemes. This alignment further supports the robustness and effectiveness of our method.

F.2. Quantifying Image-Level Reliability

This section provides an extended version of Table 3 with more methods such as the proposed method but with a fixed threshold. Furthermore, we show more results with different Perf metrics by evaluating it with AP50 and AP75 (average precision with IoU threshold 50% and 75%). The results are shown in Table 6.

As illustrated, the observation is consistent across different settings. Another notable observation is the comparison between the fixed threshold versus our adaptive threshold selection using OCE. Although the proposed fixed-threshold approach (0.3) occasionally outperforms the adaptive method, the performance gap remains marginal. Moreover, the fixed threshold consistently exhibits a lower correlation with UP-DETR, for which the optimal threshold has been empirically determined to be approximately 0.5 (0.45 by OCE and 0.55 by LRP). This indicates that although the OCE approach may not achieve threshold selection that best approximates the optimal positives, it ensures the robustness of uncertainty quantification performance. In contrast, fixed thresholding can degrade performance when the chosen value deviates from the optimal threshold.

Finally, we perform an ablation study on the scaling factor (λ), with the results presented in Figure 8. The study shows that the optimal scaling factor lies within the range of 5.0 to 10.0. Notably, this range remains effective even for out-of-distribution datasets, such as Cityscapes and Foggy Cityscapes. This consistency suggests that the scaling factor selected using the validation set (e.g., COCO) generalizes well across datasets. Furthermore, it demonstrates that ContrastiveConf with $\lambda > 0.0$ consistently outperforms Conf⁺ (i.e., $\lambda = 0.0$).

G. Comparative Study on Post-Processing

In this section, we provide a comprehensive analysis regarding the impact of post-processing on the model’s overall calibration quality. First, we vary the hyperparameter of the standard post-processing processes. In this first analysis, to exclude the dependency of the final performance on OCE, we don’t use OCE as a selection criterion. Rather, we choose the best hyperparameter on the validation set for each setting and compare their best-possible performances. The results are shown in Table 7.

As illustrated, we can observe that the confidence thresholding approach outperforms the top- k and NMS approaches. Top- k achieves the minimum OCE with top-20. Given that the average and 95th percentile number of objects per image in the COCO dataset are 7 and 22, respectively, these results appear reasonable. Therefore, we confirm that using an excessively large number (e.g., 100) for top- k is inadequate for achieving well-calibrated predictions.

Similarly, we compare the image-level uncertainty quantification performance, and the results are shown in Table 8. We reconfirm the effectiveness of confidence thresholding; for Deformable-DETR, Cal-DETR, and DINO, the optimal thresholds are approximately 0.3, aligning well with values commonly employed in previous studies. For UP-DETR, the optimal thresholds exceed 0.5, highlighting the potential limitation of using a fixed threshold in image-level UQ applications. Moreover, the correlation is negative especially when NMS is applied along with the Conf⁺ framework. This is because, while most of the optimal positive queries are likely to be included with NMS, a substantial number of optimal negative queries remain within the final subset, often outnumbering the positive ones by several times. As a result, applying NMS leads to an inaccurate reliability assessment. However, many schemes, including NMS, achieve significant improvement when used with the proposed contrastive framework. This is because even if the post-processing scheme is inaccurate, the framework can robustly perform by leveraging the negative queries.

Lastly, we plot the OCE and image-level UQ performance with different hyperparameter selections to show the sensitivity of each scheme to the choice of hyperparameter. As depicted in Figure 10, the empirical results highlight that **carefully identifying a reliable subset is crucial for achieving both high object-level calibration quality and effective image-level uncertainty quantification performance**. We also highlight this claim with an exemplary visualization in Figure 9.

Table 5. Comparison of the effectiveness of the proposed OCE and baseline metrics, focusing on their ranking correlation with the rankings given by the models’ calibration quality on optimal positive predictions (denoted by the superscript *). For each metric, various post-processing schemes (i.e., ways to identify positive predictions) are applied and indicated within parentheses. Correlations exceeding 0.9 are highlighted in blue, while negative correlations are highlighted in red. Our OCE-based rankings consistently provide strong correlations with optimal ranking and OCE effectively measures the model’s calibration quality alongside the post-processing scheme employed.

Methods	COCO (in-distribution)			Cityscapes (near OOD)			Foggy Cityscapes (OOD)			Average	
	D-ECE*	LA-ECE ₀ *	OCE*	D-ECE*	LA-ECE ₀ *	OCE*	D-ECE*	LA-ECE ₀ *	OCE*		
References	D-ECE*	1.000	0.995	0.969	1.000	0.996	0.993	1.000	0.873	0.996	0.980 ± 0.039
	LA-ECE ₀ *	0.995	1.000	0.948	0.996	1.000	0.990	0.873	1.000	0.836	0.960 ± 0.059
	OCE _{ENS} *	0.969	0.948	1.000	0.993	0.990	1.000	0.996	0.836	1.000	0.970 ± 0.050
Baselines	AP (Top-100) [6, 14]	0.552	0.583	0.343	0.779	0.784	0.700	0.597	0.843	0.523	0.634 ± 0.149
	AP@50 (Top-100) [14]	0.380	0.409	0.164	0.687	0.710	0.606	-0.360	0.079	-0.440	0.249 ± 0.402
	AP@75 (Top-100) [14]	0.652	0.680	0.458	0.830	0.829	0.757	0.765	0.930	0.705	0.734 ± 0.127
	LRP (LRP) [18]	0.103	0.051	0.338	-0.268	-0.272	-0.150	-0.257	-0.610	-0.170	-0.137 ± 0.257
	D-ECE (D-ECE)	-0.757	-0.700	-0.772	0.365	0.284	0.337	0.309	0.436	0.336	-0.018 ± 0.514
	D-ECE (Top-100)	-0.873	-0.833	-0.966	0.608	0.576	0.511	-0.254	0.250	-0.316	-0.144 ± 0.614
	D-ECE (0.3) [10]	0.905	0.939	0.827	0.982	0.967	0.990	0.964	0.799	0.981	0.928 ± 0.067
	D-ECE (LRP)	0.802	0.855	0.659	0.987	0.984	0.999	0.983	0.793	0.996	0.895 ± 0.116
	D-ECE (OCE _{ENS})	0.856	0.901	0.727	0.987	0.983	0.999	0.983	0.793	0.996	0.914 ± 0.095
	LA-ECE ₀ (LA-ECE ₀)	-0.960	-0.930	-0.968	-0.913	-0.874	-0.907	-0.826	-0.839	-0.835	-0.895 ± 0.051
	LA-ECE ₀ (Top-100)	-0.944	-0.913	-0.994	-0.431	-0.482	-0.517	-0.786	-0.386	-0.822	-0.697 ± 0.228
	LA-ECE ₀ (0.3)	-0.789	-0.729	-0.842	-0.780	-0.818	-0.830	-0.451	-0.041	-0.468	-0.639 ± 0.254
	LA-ECE ₀ (LRP) [11]	-0.908	-0.864	-0.948	-0.833	-0.877	-0.846	-0.901	-0.597	-0.913	-0.854 ± 0.097
	LA-ECE ₀ (OCE _{ENS})	-0.901	-0.855	-0.943	-0.723	-0.780	-0.739	-0.884	-0.568	-0.897	-0.810 ± 0.112
Ours	OCE _{ENS} (OCE _{ENS})	0.962	0.940	1.000	0.987	0.983	0.999	0.964	0.737	0.984	0.951 ± 0.078
	OCE _{MAX} (OCE _{MAX})	0.954	0.929	0.998	0.954	0.958	0.983	0.955	0.697	0.976	0.934 ± 0.086

Table 6. Comparison of the proposed method (ContrastiveConf) with baseline methods on their Pearson correlation coefficient with the image-level reliability in Equation (6), with different models. Perf is evaluated using AP (top), AP50 (middle), and AP75 (bottom) metrics. For each model, we apply the optimal matching, the standard post-processing scheme (Top-100 and confidence thresholding by 0.3), and the proposed OCE-based post-processing scheme, as indicated within the parentheses. The strongest correlations are highlighted in bold, while negative correlations appear in red. First, the proposed method achieves the highest correlation with image-level reliability. In addition, it is noteworthy that the average confidence of negative predictions (Conf^-) exhibits a negative correlation with image-level reliability, in contrast to the positive correlation observed when using positive predictions (Conf^+). Although the proposed fixed-threshold approach (0.3) occasionally outperforms the adaptive method, the performance gap remains marginal. Moreover, the fixed threshold consistently exhibits lower correlation with UP-DETR, for which the optimal threshold has been empirically determined to be approximately 0.5.

Methods	COCO (in-distribution)				Cityscapes (near OOD)				Foggy Cityscapes (OOD)				
	UP-DETR	D-DETR	Cal-DETR	DINO	UP-DETR	D-DETR	Cal-DETR	DINO	UP-DETR	D-DETR	Cal-DETR	DINO	
Oracles	Conf ⁺ (Optimal)	0.503	0.618	0.670	0.635	0.555	0.647	0.649	0.633	0.561	0.642	0.662	0.634
	Conf ⁻ (Optimal)	-0.608	-0.584	-0.572	-0.586	-0.293	-0.296	-0.330	-0.311	-0.177	-0.235	-0.212	-0.196
	ContrastiveConf (Optimal)	0.700	0.684	0.709	0.695	0.601	0.633	0.662	0.634	0.612	0.657	0.672	0.643
Baselines	Conf ⁺ (Top-100)	-0.619	-0.603	-0.581	-0.601	-0.409	-0.374	-0.372	-0.391	-0.262	-0.270	-0.239	-0.229
	Conf ⁺ (0.3)	0.476	0.464	0.539	0.504	0.229	0.353	0.385	0.399	0.195	0.256	0.258	0.258
Ours	Conf ⁺ (OCE)	0.442	0.477	0.547	0.512	0.237	0.355	0.393	0.370	0.228	0.291	0.270	0.274
	Conf ⁻ (OCE)	-0.633	-0.581	-0.571	-0.585	-0.365	-0.389	-0.379	-0.394	-0.245	-0.325	-0.253	-0.283
	ContrastiveConf (OCE)	0.585	0.570	0.597	0.587	0.334	0.432	0.431	0.438	0.287	0.362	0.302	0.327
	ContrastiveConf (0.3)	0.568	0.574	0.599	0.594	0.297	0.437	0.430	0.464	0.248	0.346	0.296	0.325
	ContrastiveConf (Top-100)	-0.619	-0.253	-0.490	-0.321	-0.409	-0.342	-0.358	-0.360	-0.262	-0.175	-0.215	-0.139

(a) AP

Methods	COCO (in-distribution)				Cityscapes (near OOD)				Foggy Cityscapes (OOD)				
	UP-DETR	D-DETR	Cal-DETR	DINO	UP-DETR	D-DETR	Cal-DETR	DINO	UP-DETR	D-DETR	Cal-DETR	DINO	
Oracles	Conf ⁺ (Optimal)	0.488	0.591	0.637	0.611	0.584	0.638	0.616	0.642	0.598	0.640	0.624	0.639
	Conf ⁻ (Optimal)	-0.583	-0.580	-0.555	-0.575	-0.248	-0.305	-0.316	-0.324	-0.137	-0.185	-0.175	-0.156
	ContrastiveConf (Optimal)	0.675	0.664	0.677	0.673	0.594	0.630	0.629	0.646	0.629	0.634	0.629	0.632
Baselines	Conf ⁺ (Top-100)	-0.586	-0.581	-0.546	-0.571	-0.375	-0.369	-0.351	-0.394	-0.216	-0.217	-0.196	-0.204
	Conf ⁺ (0.3)	0.445	0.435	0.494	0.465	0.229	0.321	0.342	0.379	0.203	0.223	0.179	0.194
Ours	Conf ⁺ (OCE)	0.426	0.443	0.501	0.471	0.242	0.331	0.349	0.364	0.256	0.239	0.198	0.211
	Conf ⁻ (OCE)	-0.600	-0.576	-0.554	-0.573	-0.317	-0.394	-0.357	-0.406	-0.194	-0.277	-0.216	-0.247
	ContrastiveConf (OCE)	0.560	0.545	0.554	0.552	0.314	0.416	0.388	0.438	0.285	0.302	0.229	0.263
	ContrastiveConf (0.3)	0.532	0.553	0.557	0.561	0.277	0.418	0.388	0.456	0.237	0.298	0.216	0.259
	ContrastiveConf (Top-100)	-0.586	-0.189	-0.435	-0.250	-0.375	-0.315	-0.332	-0.340	-0.216	-0.122	-0.171	-0.121

(b) AP@50

Methods	COCO (in-distribution)				Cityscapes (near OOD)				Foggy Cityscapes (OOD)				
	UP-DETR	D-DETR	Cal-DETR	DINO	UP-DETR	D-DETR	Cal-DETR	DINO	UP-DETR	D-DETR	Cal-DETR	DINO	
Oracles	Conf ⁺ (Optimal)	0.490	0.593	0.629	0.598	0.486	0.586	0.608	0.563	0.488	0.607	0.635	0.574
	Conf ⁻ (Optimal)	-0.572	-0.541	-0.521	-0.538	-0.280	-0.244	-0.284	-0.274	-0.154	-0.234	-0.182	-0.189
	ContrastiveConf (Optimal)	0.672	0.649	0.662	0.649	0.541	0.562	0.614	0.563	0.534	0.627	0.641	0.587
Baselines	Conf ⁺ (Top-100)	-0.580	-0.555	-0.523	-0.549	-0.373	-0.314	-0.325	-0.348	-0.226	-0.266	-0.206	-0.216
	Conf ⁺ (0.3)	0.459	0.434	0.497	0.467	0.214	0.320	0.348	0.351	0.188	0.231	0.290	0.241
Ours	Conf ⁺ (OCE)	0.423	0.447	0.503	0.478	0.234	0.330	0.361	0.322	0.206	0.272	0.293	0.262
	Conf ⁻ (OCE)	-0.597	-0.539	-0.520	-0.537	-0.339	-0.325	-0.327	-0.342	-0.220	-0.321	-0.217	-0.269
	ContrastiveConf (OCE)	0.557	0.532	0.548	0.545	0.319	0.386	0.390	0.381	0.258	0.346	0.314	0.312
	ContrastiveConf (0.3)	0.543	0.535	0.551	0.548	0.279	0.384	0.385	0.406	0.233	0.324	0.316	0.306
	ContrastiveConf (Top-100)	-0.580	-0.225	-0.435	-0.291	-0.373	-0.295	-0.320	-0.334	-0.226	-0.170	-0.188	-0.137

(c) AP@75

Table 7. Comparison of post-processing schemes based on calibration quality (i.e., OCE). We evaluated three standard methods: confidence thresholding, top- k , and NMS (without confidence thresholding). For each scheme, the optimal hyperparameter selected from the validation set is shown in parentheses, and is applied on the test set. the strongest correlations are highlighted in bold. Confidence thresholding achieves the lowest OCE, demonstrating its better efficacy compared to the other schemes. The optimal thresholds are approximately 0.3, aligning well with values commonly employed in previous studies.

Methods	COCO (in-distribution)				Cityscapes (near OOD)				Foggy Cityscapes (OOD)			
	UP-DETR	D-DETR	Cal-DETR	DINO	UP-DETR	D-DETR	Cal-DETR	DINO	UP-DETR	D-DETR	Cal-DETR	DINO
Thresholding	0.276 (0.35)	0.450 (0.20)	0.416 (0.25)	0.436 (0.25)	0.313 (0.45)	0.430 (0.30)	0.413 (0.30)	0.402 (0.35)	0.387 (0.40)	0.488 (0.30)	0.469 (0.30)	0.458 (0.30)
Top- k	0.358 (20.00)	0.485 (20.00)	0.457 (20.00)	0.479 (20.00)	0.352 (20.00)	0.451 (20.00)	0.436 (20.00)	0.422 (20.00)	0.416 (20.00)	0.500 (20.00)	0.490 (20.00)	0.473 (20.00)
NMS	0.358 (0.90)	0.535 (0.90)	0.624 (0.90)	0.521 (0.90)	0.426 (0.90)	0.625 (0.90)	0.784 (0.90)	0.583 (0.90)	0.495 (0.90)	0.650 (0.90)	0.794 (0.90)	0.609 (0.90)

Table 8. Comparison of post-processing schemes and baseline methods based on their Pearson correlation coefficients with image-level reliability when Conf^+ and ContrastiveConf are applied, respectively. We evaluated three standard methods: confidence thresholding, top- k , and NMS (without confidence thresholding). For each scheme, the optimal hyperparameter selected from the validation set is shown in parentheses, and is applied on the test set. the strongest correlations are highlighted in bold. Confidence thresholding achieves the lowest OCE, demonstrating its better efficacy compared to the other schemes. For Deformable-DETR, Cal-DETR, and DINO, the optimal thresholds are approximately 0.3, aligning well with values commonly employed in previous studies. For UP-DETR, the optimal thresholds exceed 0.5, highlighting the potential limitation of using a fixed threshold in image-level uncertainty quantification (UQ) applications.

UQ	Methods	COCO (in-distribution)				Cityscapes (near OOD)				Foggy Cityscapes (OOD)			
		UP-DETR	D-DETR	Cal-DETR	DINO	UP-DETR	D-DETR	Cal-DETR	DINO	UP-DETR	D-DETR	Cal-DETR	DINO
Conf^+	Thresholding	0.479 (0.25)	0.478 (0.20)	0.547 (0.25)	0.512 (0.25)	0.333 (0.80)	0.355 (0.25)	0.411 (0.20)	0.403 (0.35)	0.229 (0.50)	0.291 (0.25)	0.281 (0.15)	0.282 (0.35)
	Top- k	0.067 (1.00)	0.132 (1.00)	0.252 (1.00)	0.155 (1.00)	-0.037 (2.00)	0.019 (1.00)	0.078 (1.00)	0.021 (1.00)	0.080 (1.00)	-0.006 (1.00)	0.026 (1.00)	0.090 (1.00)
	NMS	-0.588 (0.10)	-0.560 (0.10)	-0.548 (0.10)	-0.562 (0.10)	-0.402 (0.10)	-0.346 (0.10)	-0.332 (0.10)	-0.365 (0.10)	-0.240 (0.10)	-0.265 (0.10)	-0.218 (0.10)	-0.224 (0.10)
ContrastiveConf	Thresholding	0.597 (0.55)	0.574 (0.30)	0.599 (0.30)	0.594 (0.30)	0.408 (0.80)	0.437 (0.30)	0.443 (0.20)	0.472 (0.35)	0.312 (0.75)	0.362 (0.25)	0.315 (0.40)	0.352 (0.35)
	Top- k	0.629 (1.00)	0.506 (1.00)	0.474 (1.00)	0.527 (1.00)	0.409 (1.00)	0.377 (1.00)	0.324 (1.00)	0.411 (1.00)	0.284 (1.00)	0.254 (1.00)	0.156 (1.00)	0.298 (1.00)
	NMS	-0.408 (0.10)	0.585 (0.10)	0.535 (0.10)	0.574 (0.10)	-0.101 (0.10)	0.368 (0.10)	0.347 (0.10)	0.373 (0.10)	-0.001 (0.10)	0.262 (0.10)	0.228 (0.10)	0.239 (0.10)

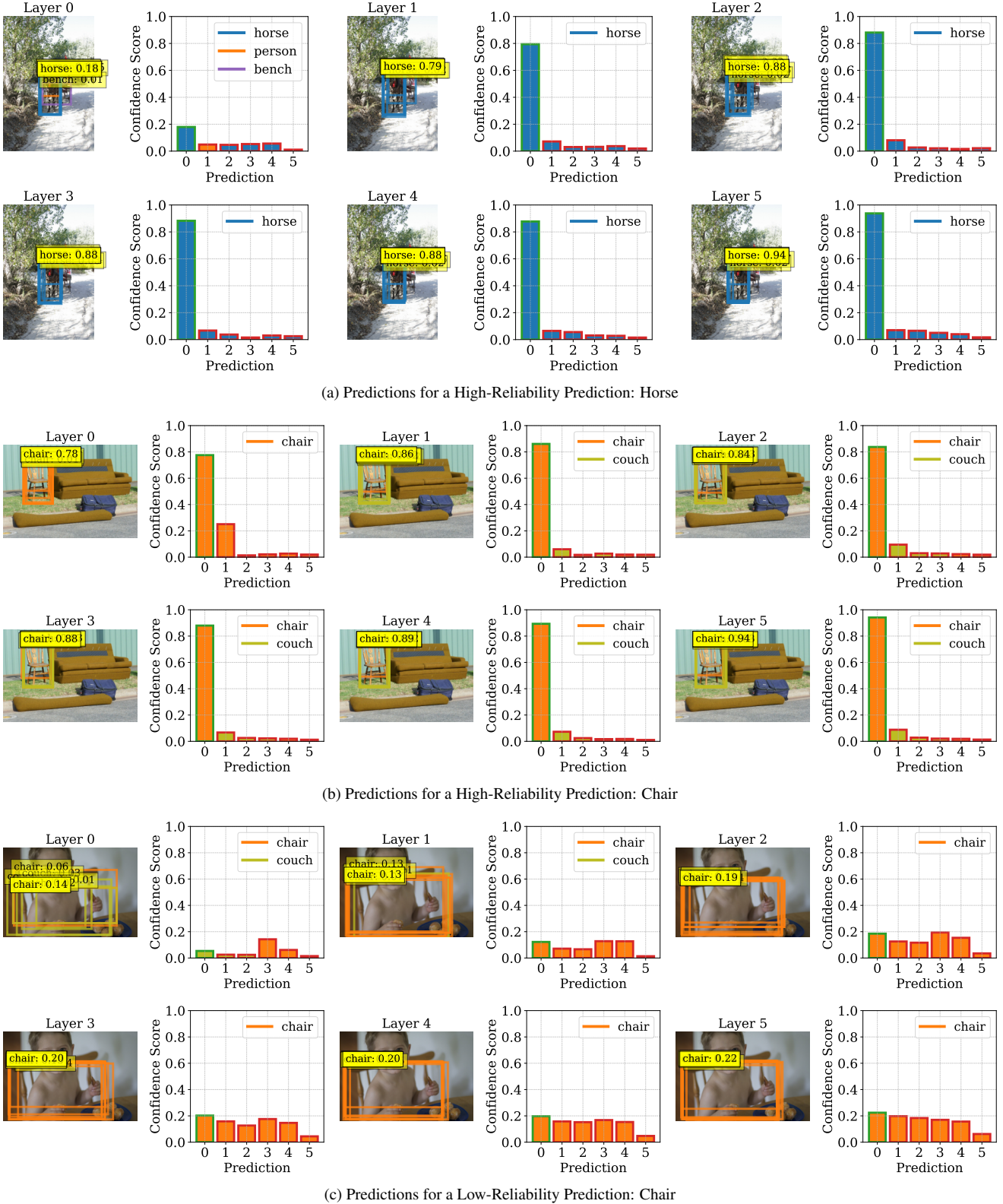
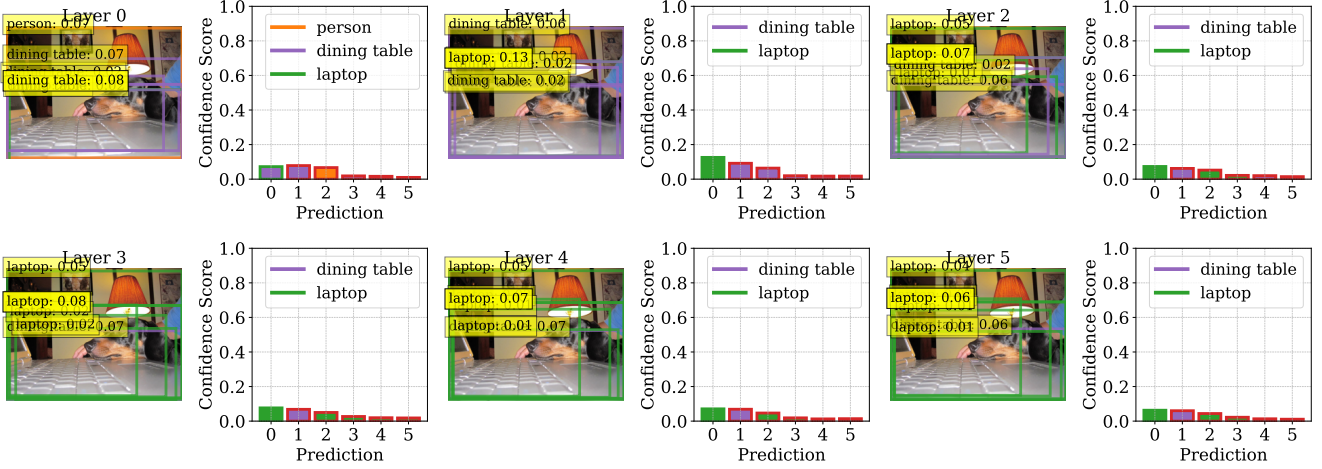
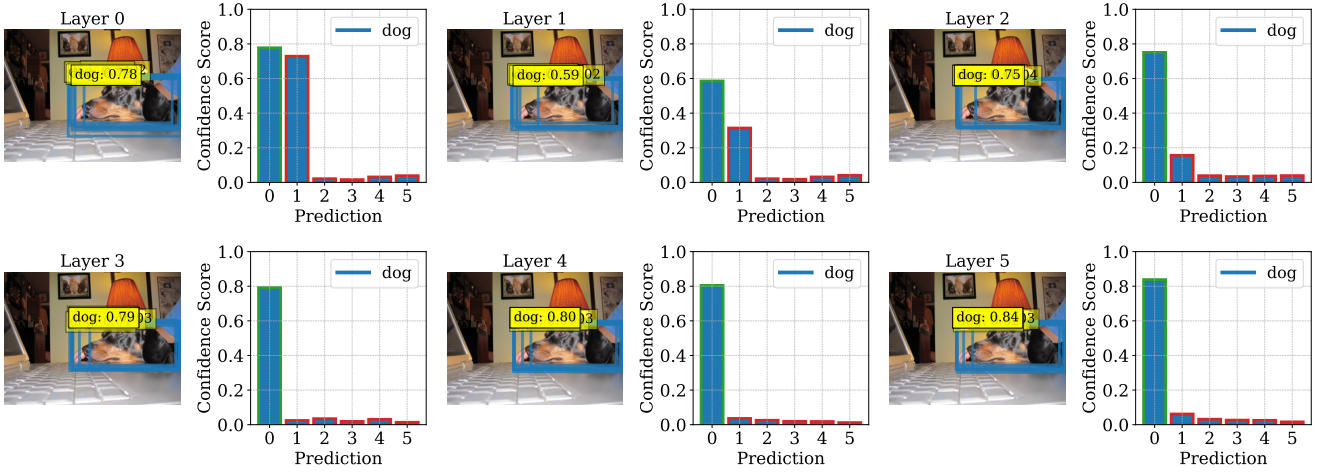


Figure 5. The evolution of predictions made by Cal-DETR across decoder layers for a high-reliability and low-reliability image. The positive query (indexed by 0 and bordered with green) and the five negative queries with the largest IoU (indexed by 1-5 and bordered with red) are presented.



(a) Predictions for a Low-Reliability Object: Laptop



(b) Predictions for a High-Reliability Object: Dog

Figure 6. The evolution of predictions made by Cal-DETR across decoder layers for two different objects (one reliable and one unreliable) in a low-reliability image. The positive query (indexed by 0 and bordered with green) and the five negative queries with the largest IoU (indexed by 1-5 and bordered with red) are presented.

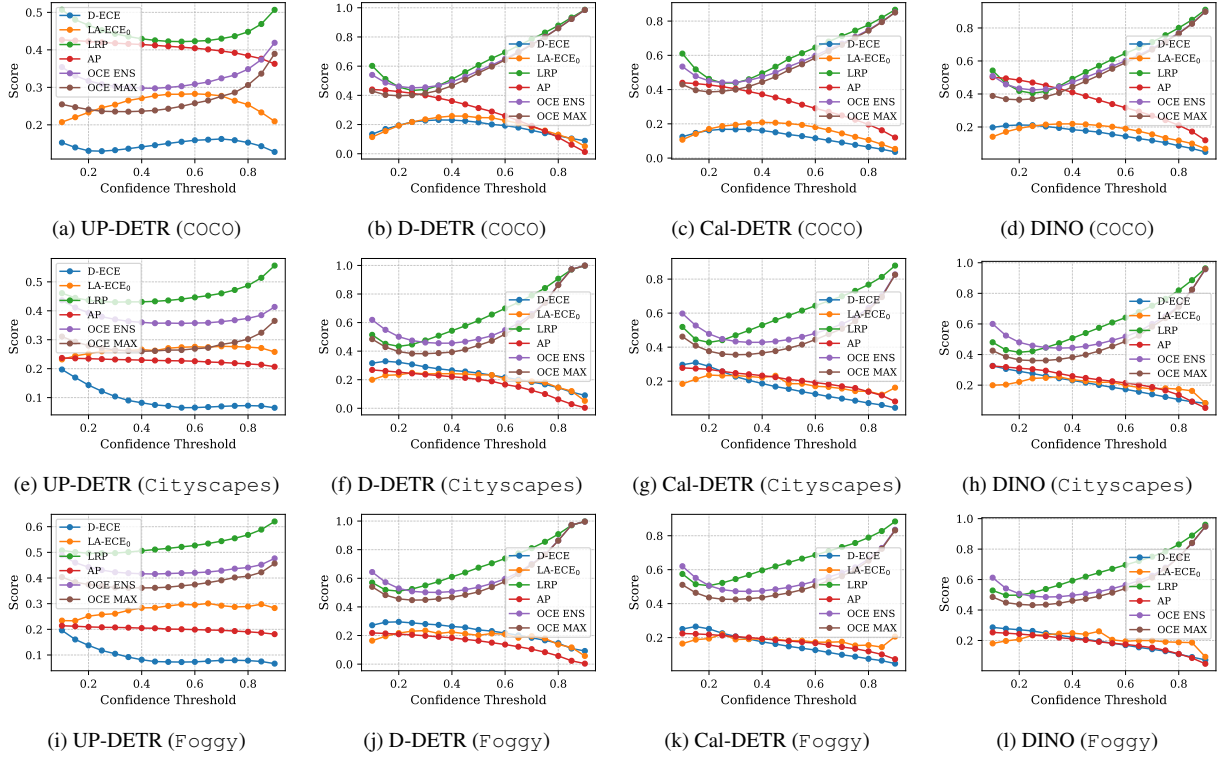


Figure 7. Impact of confidence threshold selection on various performance metrics in UP-DETR, Deformable-DETR, Cal-DETR, and DINO on COCO, Cityscapes, and Foggy Cityscapes.

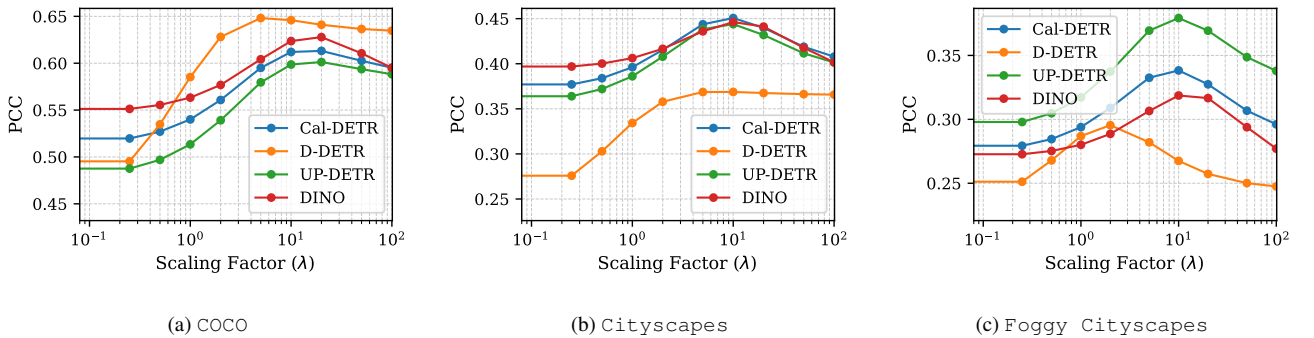


Figure 8. Impact of the scaling factor (λ) on image-level UQ performance of ContrastiveConf. Pearson correlation coefficient (PCC) using various scaling factors is reported. The optimal scaling factor lies within the range of 5.0 to 10.0, while this range generalizes well across out-of-distribution datasets. Furthermore, it shows the efficacy of ContrastiveConf over Conf⁺ (i.e., ContrastiveConf with $\lambda = 0.0$).

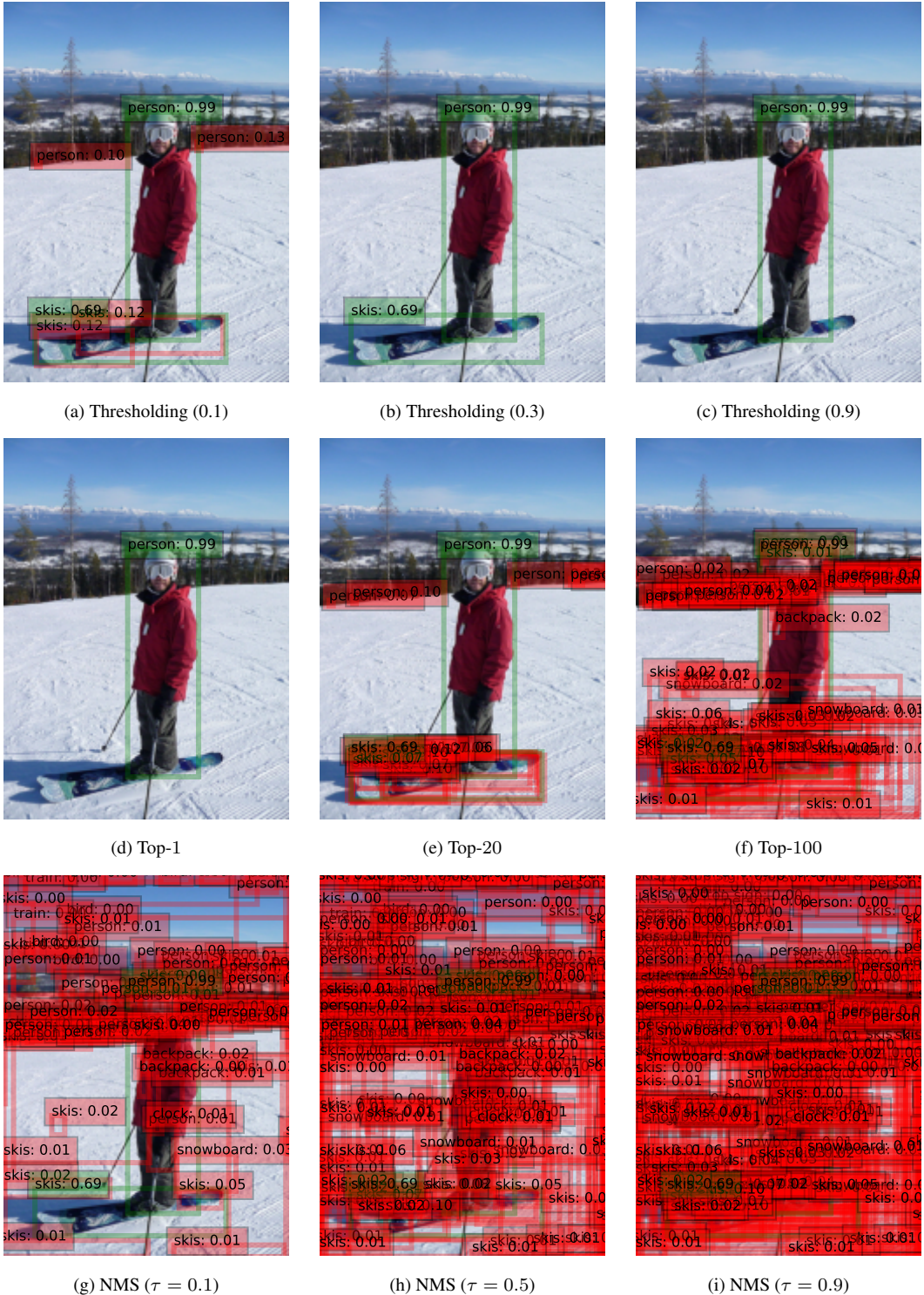


Figure 9. Exemplary visualization demonstrating the impact of parameter selection on the final subset of predictions in Cal-DETR for different post-processing schemes. Optimal positive and negative predictions are highlighted with green and red boxes, respectively. As shown, the top- k and NMS approaches often include too many negative predictions, degrading the calibration quality. Confidence thresholding with too low of a threshold faces a similar issue, while too high of a threshold risks omitting positive predictions. Therefore, accurately identifying a reliable set of predictions significantly affects the reliability of DETR for downstream applications.

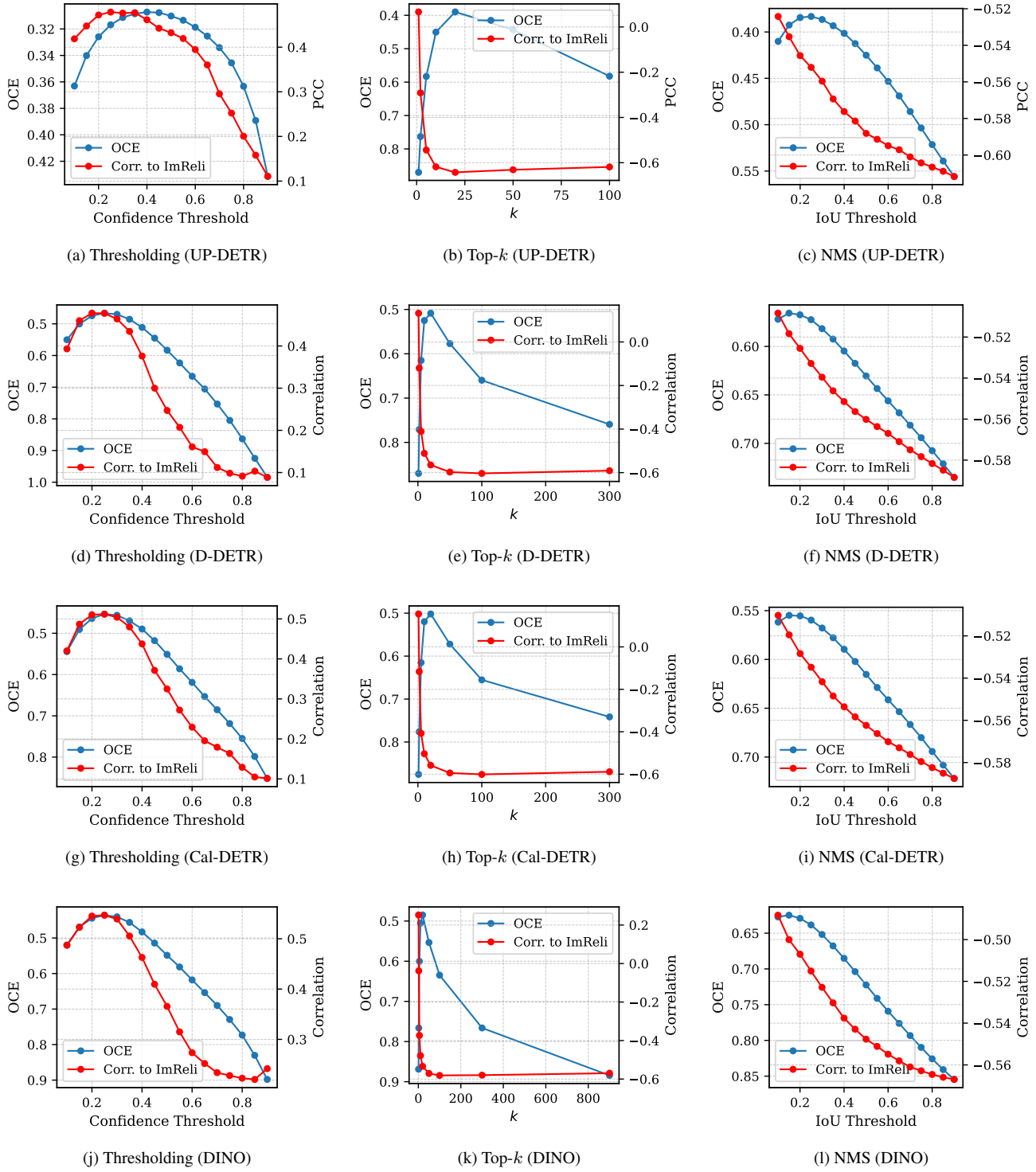


Figure 10. Impact of parameter selection on OCE (y-axis inverted) and the Pearson correlation coefficient (PCC) between ContrastiveConf and image-level reliability in Cal-DETR on COCO for different post-processing schemes.